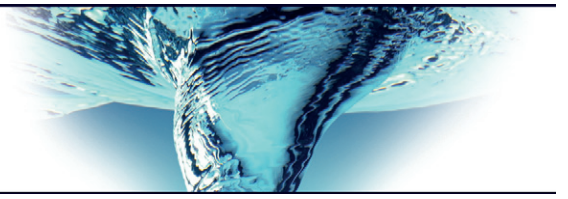
CrossMark

J. Fluid Mech. (2018), *vol.* 841, R1, doi:10.1017/jfm.2018.75



JFM RAPIDS
journals.cambridge.org/rapids

Modelling yawed wind turbine wakes: a lifting line approach

Carl R. Shapiro[1], **Dennice F. Gayme**[1] **and Charles Meneveau**[1,†]

[1]Department of Mechanical Engineering, Johns Hopkins University, Baltimore, MD 21218, USA

(Received 15 December 2017; revised 11 January 2018; accepted 11 January 2018;
first published online 20 February 2018)

Yawing wind turbines has emerged as an appealing method for wake deflection. However, the associated flow properties, including the magnitude of the transverse velocity associated with yawed turbines, are not fully understood. In this paper, we view a yawed turbine as a lifting surface with an elliptic distribution of transverse lift. Prandtl's lifting line theory provides predictions for the transverse velocity and magnitude of the shed counter-rotating vortex pair known to form downstream of the yawed turbine. The streamwise velocity deficit behind the turbine can then be obtained using classical momentum theory. This new model for the near-disk inviscid region of the flow is compared to numerical simulations and found to yield more accurate predictions of the initial transverse velocity and wake skewness angle than existing models. We use these predictions as initial conditions in a wake model of the downstream evolution of the turbulent wake flow and compare predicted wake deflection with measurements from wind tunnel experiments.

Key words: turbulent flows, wakes, wakes/jets

1. Introduction

Yawing of wind turbines has the potential to increase wind farm power production by deflecting wakes away from downstream turbines (Fleming *et al.* 2015; Bastankhah & Porté-Agel 2016; Branlard & Gaunaa 2016; Howland *et al.* 2016). Dynamic yawing can also be used to regulate wind farm power production for improved integration in power systems (Aho *et al.* 2012; Shapiro *et al.* 2017). Despite these promising emerging applications, a practical, yet accurate, aerodynamic theory is missing. Specifically, accurately predicting, from first principles, the magnitudes of the transverse velocity and the axial velocity deficit, the circulation of the shed counter-rotating vortex pair (Bastankhah & Porté-Agel 2016; Howland *et al.* 2016), and the skewness of the wake downstream remains a challenge.

Inviscid models of the region near the rotor of unyawed turbines have played an important role in wind turbine modelling. Axial momentum theory and the

† Email address for correspondence: meneveau@jhu.edu

© Cambridge University Press 2018

https://doi.org/10.1017/jfm.2018.75 Published online by Cambridge University Press

vortex cylinder model have been used to derive the celebrated Betz limit and predict the initial wake velocity deficit (Glauert 1935; Burton *et al.* 2011). Blade element momentum theory (Hansen 2008; Burton *et al.* 2011) and vortex system models (Glauert 1935; Branlard & Gaunaa 2015) have been used to predict the distribution of loads and velocity deficits in the wake. Such inviscid results are often used as initial conditions for models describing the turbulent wake downstream of the turbine (Jensen 1983; Frandsen *et al.* 2006).

In contrast, the arguments used in models of unyawed turbines cannot always be straightforwardly applied to derive accurate predictions for yawed turbines. For example, the low pressure within the cores of the counter-rotating vortices known to form downstream of a yawed turbine results in a non-vanishing transverse pressure force on the streamtube. As a result, momentum balance arguments (Jiménez, Crespo & Migoya 2010; Burton *et al.* 2011), Glauert's (1926) proposed equation for the axial induced velocity through the rotor, and the skewed elliptic vortex cylinder model (Coleman, Feingold & Stempin 1945; Branlard & Gaunaa 2016) lead to conflicting results that do not always agree with simulations. Resolving the significant differences among these models is vital for properly setting the initial conditions for models of the turbulent wake of yawed turbines.

In § 2, a model for the predominantly inviscid region near the rotor of a yawed actuator disk is proposed that agrees with measurements from numerical simulations. A key insight of this approach is to regard a yawed actuator disk as a lifting surface with an elliptic distribution of transverse lift. Then, Prandtl's lifting line theory (Milne-Thomson 1973) is used to predict the initial constant transverse velocity and the strength of the counter-rotating vortex pair. The transverse velocity is then combined with streamwise momentum theory to predict the induced velocity through the rotor and the initial streamwise velocity deficit. In § 3 these results are used as initial conditions in a model for the evolution of a turbulent wake far downstream of a yawed turbine.

2. The yawed actuator disk as an elliptically loaded lifting line

In actuator disk theories, wind turbines can be treated as porous disks that exert a thrust force perpendicular to the rotor area on the flow field. Figure 1(*a*) defines the coordinate system $\boldsymbol{x} = (x, y, z)$ with the unit vectors $\boldsymbol{i}$, $\boldsymbol{j}$, and $\boldsymbol{k}$ aligned with the incoming flow velocity $\boldsymbol{U}_\infty = U_\infty \boldsymbol{i}$. The coordinate system $\boldsymbol{x}' = (x', y', z')$ is aligned with the unit normal of the actuator disk $\boldsymbol{n} = \cos\gamma\, \boldsymbol{i} + \sin\gamma\, \boldsymbol{j}$, where γ is the angle between $\boldsymbol{U}_\infty$ and $\boldsymbol{n}$. The actuator disk forcing per unit volume $\boldsymbol{f}(\boldsymbol{x}) = T\,\mathcal{R}(\boldsymbol{x})\,\boldsymbol{n}$ equally distributes the total thrust force T in the direction $\boldsymbol{n}$, where the area fraction function is defined as $\mathcal{R}(\boldsymbol{x}) = \pi^{-1}R^{-2}\delta(x')H(R - |r'|)$, $\delta(x)$ is the Dirac delta function, $H(x)$ is the Heaviside (unit step) function, $r'^2 = y'^2 + z'^2$, and $R = D/2$ is the radius of the disk. The area fraction function is non-zero only within a disk of infinitesimal thickness that encloses the rotor swept area. The velocity field is denoted by $\boldsymbol{u}(\boldsymbol{x})$, and the fluid density is denoted by ρ. The total thrust force can be written in terms of the inflow velocity U_∞ and thrust coefficient C_T or the disk-averaged velocity normal to the disk

$$u_d = \int \boldsymbol{u}(\boldsymbol{x}) \cdot \boldsymbol{n}\, \mathcal{R}(\boldsymbol{x})\, d^3\boldsymbol{x}, \tag{2.1}$$

and local thrust coefficient C_T' (Calaf, Meneveau & Meyers 2010) as follows

$$T = -\tfrac{1}{2}\rho\pi R^2 C_T U_\infty^2 \cos^2\gamma = -\tfrac{1}{2}\rho\pi R^2 C_T' u_d^2. \tag{2.2}$$

https://doi.org/10.1017/jfm.2018.75 Published online by Cambridge University Press

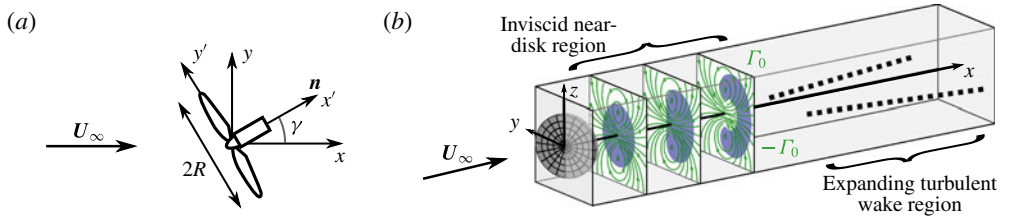


FIGURE 1. (*a*) An actuator disk with radius R yawed at an angle γ. (*b*) Sketch of the two regions downstream of the rotor: the inviscid region of streamwise velocity deficit, shown in blue, with a counter-rotating vortex pair with circulation $\pm\Gamma_0$, superimposed in green, and the expanding turbulent wake region, shown as dashed lines, developing downstream of the inviscid near-disk region.

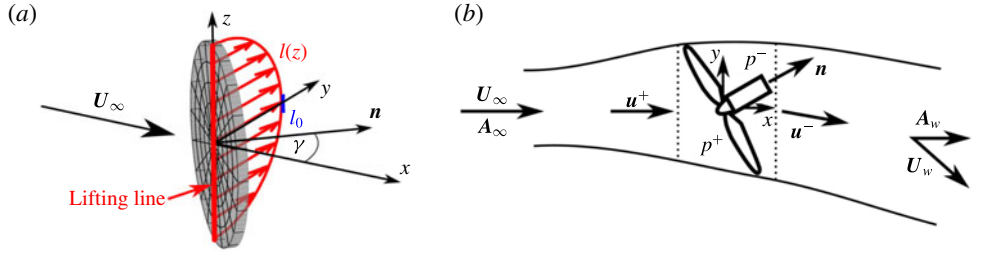


FIGURE 2. (*a*) The lifting line segment through the origin between $z=-R$ and $z=R$ has a lift force per unit span of $l(z)$. At $z=0$ the lift is l_0 and the circulation is Γ_0. (*b*) The inviscid streamtube in the near-rotor region of a yawed actuator disk. The rotor region, assumed to be an elliptic cylinder, is between the dotted lines.

As in models of the flow around unyawed actuator disks, we divide the flow into two regions, as shown in figure 1(*b*). We first consider the predominantly inviscid region near the disk. The description of this region can then be used as an initial condition for models of the wake, where turbulent mixing dominates, as discussed in § 3. In the inviscid region, we first employ the vorticity equation to avoid dealing with pressure fields. In the present context, examining vorticity transport is equivalent to considering the fate of circulation.

The appropriate framework is the Prandtl lifting line theory (Milne-Thomson 1973), which can be used to predict the transverse velocity, shed circulation, and strength of the counter-rotating vortex pair. To facilitate the use of the Prandtl lifting line theory, we decompose the thrust force into a streamwise force along the x-axis and a transverse force along the y-axis, which we refer to as the 'transverse lift'. The yawed actuator disk can be viewed as an inclined lift-generating surface, akin to an airfoil, with a total span of $2R$ and a chord length $c(z)$ that varies along the vertical direction z. Geometrically, the chord length $c(z)$ is the length of the line segment between the two outer points of the disk at a point z, expressed mathematically as $[c(z)/2]^2+z^2=R^2$. To apply lifting line theory, the associated lift force can be thought to be distributed along a line segment through the origin between $z=-R$ and $z=R$, as shown in figure 2(*a*). The lift distribution imposed by the fluid on the actuator disk is assumed to be uniformly distributed over the disk as

$$L\mathcal{R}(\boldsymbol{x})\,\boldsymbol{j}=-T\sin\gamma\,\mathcal{R}(\boldsymbol{x})\,\boldsymbol{j}, \tag{2.3}$$

https://doi.org/10.1017/jfm.2018.75 Published online by Cambridge University Press

where L is the total lift force and $\mathcal{R}(\boldsymbol{x})$ is the area fraction function described above. Therefore, the lift per unit span $l(z) = (L/\pi R^2)c(z)$ is equal to the lift per unit area times the chord length. Using the geometric relationship $[c(z)/2]^2 + z^2 = R^2$, the resulting distribution of circulation along the span $\Gamma(z)$, which is related to the lift by $l(z) = -\rho U_\infty \Gamma(z)$, has an elliptic distribution

$$\frac{\Gamma^2(z)}{\Gamma_0^2} + \frac{z^2}{R^2} = 1, \tag{2.4}$$

with a maximum circulation magnitude at $z = 0$. At $z = 0$ the chord length is $c_0 = 2R$, the lift is $l_0 = 2L/(\pi R) = -2T \sin\gamma/(\pi R)$, and the circulation is

$$\Gamma_0 = -\frac{l_0}{\rho U_\infty} = -R\, C_T U_\infty \cos^2\gamma \sin\gamma. \tag{2.5}$$

According to lifting line theory (Milne-Thomson 1973), vortex filaments with a strength per unit span $\mathrm{d}\Gamma/\mathrm{d}z$ are shed and roll up into counter-rotating trailing vortices at the top and bottom of the disk with strength

$$\Gamma_{bottom} = -\Gamma_{top} = \int_{-R}^{0} \frac{\mathrm{d}\Gamma}{\mathrm{d}z}\,\mathrm{d}z = \Gamma_0. \tag{2.6}$$

An elliptic lift distribution is special because it induces a constant transverse velocity (downwash) given by (Milne-Thomson 1973)

$$\delta v_0 = -\frac{\Gamma_0}{4R} = \frac{1}{4} C_T U_\infty \cos^2\gamma \sin\gamma. \tag{2.7}$$

Equations (2.5) and (2.7) thus define the transverse behaviour of the inviscid region.

In order to provide data to test predictions based on the proposed model in (2.4)–(2.7), numerical simulations of flow around a yawed actuator disk under uniform, laminar inflow are carried out using the pseudo-spectral code LESGO, which was validated in prior works (e.g. Calaf *et al.* 2010; Stevens, Martínez & Meneveau 2018). A yawed actuator disk of diameter D is placed in a domain of length $L_x = 11.52D$ and cross-section size $L_y = L_z = 5.76D$ using a total of $384 \times 192 \times 192$ grid points. The centre of the actuator disk is placed in the centre of a y–z plane $3.6D$ downstream of the domain inlet. A uniform inflow velocity U_∞ is applied using a fringe region forcing (Stevens, Graham & Meneveau 2014). Molecular viscosity is neglected and the Smagorinsky model is used for numerical stability with $C_s = 0.16$. Since the flow in the bulk of the near-disk region of interest remains laminar and inviscid and the effect of the subgrid model is confined to the thin shear layer at the boundary of the wake, which is not included in the subsequent analysis, the details of the subgrid modelling are not important for present purposes. The simulations are insensitive to the choice of C_s, yielding the same results for $C_s = 0.08$. Various yaw angles γ are considered. LESGO uses the local formulation of the thrust force with a local thrust coefficient C_T' (Calaf *et al.* 2010). The force is applied using the area fraction function filtered by a three-dimensional Gaussian with a filter width $\sigma_{\mathcal{R}} = 1.5h/\sqrt{12}$ proportional to the grid size $h = (\Delta x^2 + \Delta y^2 + \Delta z^2)^{1/2}$, where Δx, Δy, and Δz are the grid spacings.

Representative results at downstream distances $x/D = 1$, 2, and 3 are shown in figure 3 for $C_T' = 1.33$ and $\gamma = 30°$. A wake that stays laminar for a large portion of

https://doi.org/10.1017/jfm.2018.75 Published online by Cambridge University Press

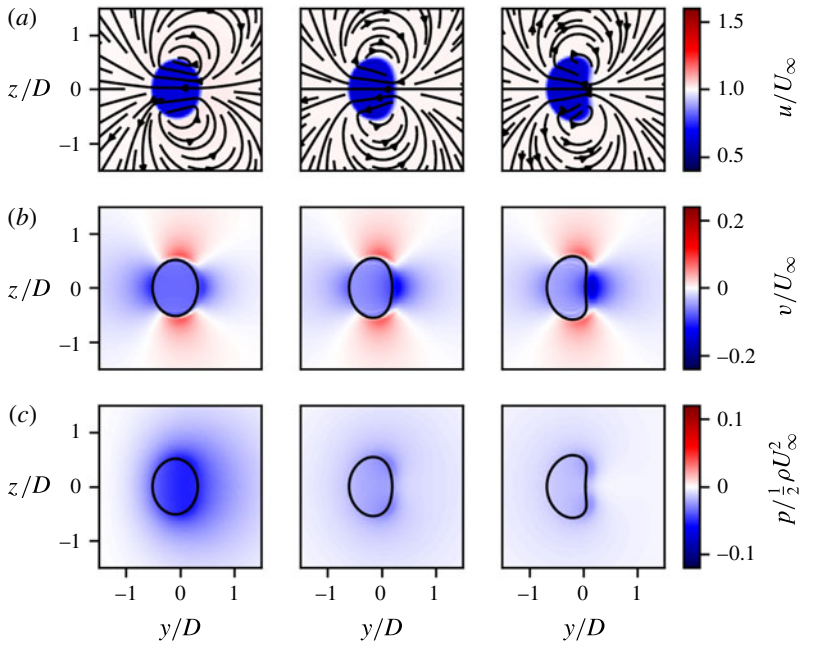


FIGURE 3. Simulation results for $C_T' = 1.33$ and yaw angle $\gamma = 30°$ in a domain $L_x/D = 11.52$ and $L_y/D = L_z/D = 5.76$. Shown are colour contours of (*a*) streamwise velocity, (*b*) transverse velocity, and (*c*) pressure at downstream locations $x/D = 1$, 2, and 3, respectively. Panel (*a*) includes streamlines in the y–z plane. The transverse velocity and pressure plots show the outline of the wake, defined by the streamtube that passes the rotor at a radius of $r' = 0.9R$.

the domain is generated by the actuator disk forcing. At $x/D = 1$ near the actuator disk, the wake forms an ellipse with uniform streamwise and transverse velocity components inside of the wake. The transverse component of the force generates the well-known counter-rotating vortex pair (Howland *et al.* 2016; Bastankhah & Porté-Agel 2016), which curls the wake as it moves downstream, shown schematically in figure 1(*b*).

Further simulations are performed at yaw angles $\gamma = 10°$, 20°, 30°, and 40° and local thrust coefficients $C_T' = 0.8$, 1.0, and 1.33. From these simulations, the spanwise circulation distribution $\Gamma(z)$ is evaluated numerically via integration along rectangular contours running from the inlet of the domain to $x = R$ and spanning the entire width of the domain. The circulation of each shed vortex Γ_0 is calculated at $x = R$ by averaging the circulation around two rectangular circuits spanning $|y| \leqslant 3R$ and $|z| \leqslant 3R$.

We seek to compare the measured results to (2.4) and (2.5), for which the disk radius is an important parameter. The footprint of the applied force in the simulations extends slightly from the geometrically prescribed disk dimensions, owing to the use of a filtered area fraction function. To correct for the filtered geometric representation of the disk, the width of an equivalent top-hat filter (Pope 2000) $\sqrt{12}\sigma_{\mathcal{R}} = 1.5h$ ($h \ll R$ is the grid size) is added to the diameter of the disk in (2.4) when applying the inviscid model. The resulting effective radius is $R_* = R + 0.75h$, which leads to the predicted maximum circulation being given

https://doi.org/10.1017/jfm.2018.75 Published online by Cambridge University Press

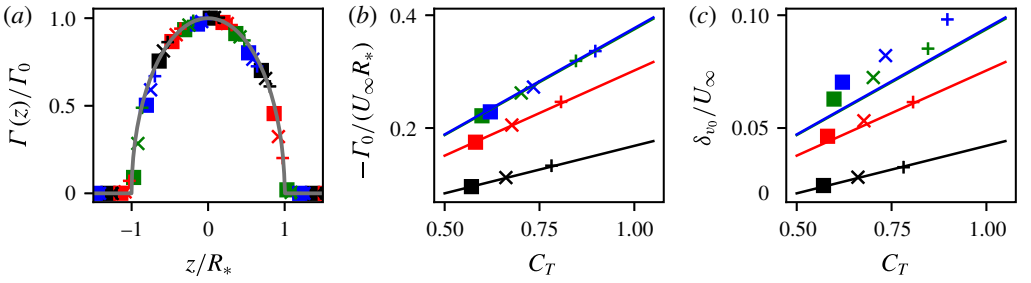


FIGURE 4. Comparisons of (*a*) the measured circulation around the actuator disk (symbols) and the expected distribution from the elliptic lifting line $(1 - z^2/R_*^2)^{1/2}$ (grey line), (*b*) the shed circulation of counter-rotating vortices measured at $x = R$ (symbols) and predicted by lifting line theory (lines), and (*c*) the maximum y–z planar-averaged transverse velocity measured in the streamtube (symbols) and transverse velocity predicted by lifting line theory (lines). Simulations are conducted with $\gamma = 10°$ (black), 20° (red), 30° (green), and 40° (blue) and $C_T' = 0.8$ (■), 1.0 (×), and 1.33 (+). The theoretical values for $\gamma = 30°$ and 40° overlap in (*b*) and (*c*).

by $\Gamma_0 = -(R + 0.75h)\, C_T U_\infty \cos^2\gamma \sin\gamma$. The thrust coefficient is obtained from $C_T = C_T' u_d^2/(U_\infty \cos\gamma)^2$, where the disk-averaged velocity u_d is measured in the simulations. As seen in the comparison shown in figures 4(*a*,*b*), the predicted circulation distribution and simulation results collapse for all γ and C_T' values tested.

Next we compare the transverse velocity magnitude δv_0 with the model. To measure this value from simulations we take the maximum y–z planar-averaged transverse velocity in the wake. The wake is defined as the streamtube passing through the disk at $r' = 0.9R$ to avoid including the thin shear layer near the actuator disk perimeter (results are quite insensitive to this choice). The downstream position of maximum transverse wake velocity occurs very near the disk, at $x \approx R$. Using the thrust coefficient obtained from $C_T = C_T' u_d^2/(U_\infty \cos\gamma)^2$, we compare $\delta v_0 = \frac{1}{4} C_T U_\infty \cos^2\gamma \sin\gamma$ to simulation measurements in figure 4(*c*). Again, excellent agreement is observed for various γ and C_T' combinations, with a slight underestimate at large γ.

In addition to the transverse velocity derived, additional expressions are needed to fully describe the inviscid region near the yawed actuator disk. The induced velocity through the disk, as well as the streamwise velocity deficit in the wake, are derived using an approach similar to the unyawed momentum theory (Glauert 1935; Burton *et al.* 2011). The streamtube through the rotor is used as a control volume and the velocity is assumed to be uniform across every cross-section, as shown in figure 2(*b*). The velocities upstream of the rotor and at the end of the inviscid region (beginning of the wake) are denoted by $\boldsymbol{U}_\infty$ and $\boldsymbol{U}_w$, respectively. Also, at those locations we consider flow through vertical sections with area vectors, $\boldsymbol{A}_\infty = A_\infty \boldsymbol{i}$ and $\boldsymbol{A}_w = A_w \boldsymbol{i}$, defined in figure 2(*b*). The disk-averaged velocity u_d through the disk area $A_d = \pi R^2$ and mass conservation yields $u_d A_d = \boldsymbol{U}_\infty \cdot \boldsymbol{A}_\infty = \boldsymbol{U}_w \cdot \boldsymbol{A}_w$, where the dots indicate inner products. The wake velocity is written as $\boldsymbol{U}_w = (U_\infty - \delta u_0)\boldsymbol{i} - \delta v_0\, \boldsymbol{j}$, where δu_0 is the streamwise velocity deficit and δv_0 is the transverse velocity magnitude specified by the lifting line theory in (2.7).

The region of the streamtube cut by the actuator disk is treated as an elliptic cylinder with a cross-sectional area of $A_d \cos\gamma$. Inside this volume, the upstream

https://doi.org/10.1017/jfm.2018.75 Published online by Cambridge University Press

and downstream pressure are assumed to be constant at p^+ and p^-, respectively. The upstream and downstream velocities are respectively $\boldsymbol{u}^+ = u_d \cos^{-1}\gamma\, \boldsymbol{i}$ and $\boldsymbol{u}^- = u_d \cos^{-1}\gamma \boldsymbol{i} - \delta v_0\, \boldsymbol{j}$. The streamwise velocity through this region is assumed to be constant and is determined using mass conservation. The transverse velocity has a discontinuity at the disk, jumping from zero to the downwash $-\delta v_0$ behind the rotor region.

Assuming that the streamwise pressure force vanishes over the streamtube's surface, as in the unyawed case (Glauert 1935), the streamwise momentum equation is

$$-\rho\, \boldsymbol{U}_\infty \cdot \boldsymbol{A}_\infty\, U_\infty + \rho\, \boldsymbol{U}_w \cdot \boldsymbol{A}_w\, (U_\infty - \delta u_0) = T\cos\gamma. \tag{2.8}$$

The Bernoulli equation is then applied from far upstream to where $p = p^+$ and from where $p = p^-$ to further downstream of the turbine where p recovers and the turbulent wake begins, as shown in figure 2(*b*). Assuming that δv_0 remains constant in the downstream part of the inviscid region, we write

$$\frac{1}{2}U_\infty^2 = \frac{1}{2}\left(\frac{u_d}{\cos\gamma}\right)^2 + \frac{p^+}{\rho}, \tag{2.9a}$$

$$\frac{1}{2}\left(\frac{u_d}{\cos\gamma}\right)^2 + \frac{1}{2}\delta v_0^2 + \frac{p^-}{\rho} = \frac{1}{2}(U_\infty - \delta u_0)^2 + \frac{1}{2}\delta v_0^2. \tag{2.9b}$$

Subtracting the two equations in (2.9), and noting that the pressure force opposes the streamwise thrust force (drag) $(p^+ - p^-)A_d = -T$, we obtain

$$\frac{1}{2}U_\infty^2 - \frac{1}{2}(U_\infty - \delta u_0)^2 = -\frac{T}{\rho A_d}. \tag{2.10}$$

Substituting the thrust force (2.2) and mass flow rate into (2.8) and (2.10) yields two equations for the unknown disk-averaged velocity and streamwise velocity deficit

$$2\frac{u_d}{U_\infty}\frac{\delta u_0}{U_\infty} = C_T\cos^3\gamma, \quad \frac{\delta u_0}{U_\infty}\left(2 - \frac{\delta u_0}{U_\infty}\right) = C_T\cos^2\gamma. \tag{2.11a,b}$$

Written in terms of the induction factor a, the solution is

$$u_d/U_\infty = \cos\gamma\,(1-a), \quad \delta u_0/U_\infty = 2a, \tag{2.12a,b}$$

where the thrust coefficient is related to the induction factor by $C_T\cos^2\gamma = 4a(1-a)$. The induction factor can subsequently be written in terms of both the standard and local thrust coefficients using the identity $C_T U_\infty^2\cos^2\gamma = C_T' u_d^2$ according to

$$a = \frac{C_T'\cos^2\gamma}{4 + C_T'\cos^2\gamma} = \frac{1}{2}\left(1 - \sqrt{1 - C_T\cos^2\gamma}\right). \tag{2.13}$$

The initial skewness angle is obtained from $\tan\alpha = -\delta v_0/(U_\infty - \delta u_0)$.

The disk-averaged velocity, streamwise velocity deficit, transverse velocity, and skewness angle of the initial wake obtained from numerical simulations, the present model, and prior models are compared in figure 5. The velocity deficit δu_0 at the end of the inviscid region is obtained from the simulations as the maximum y–z planar-averaged streamwise velocity deficit in the wake, which occurs at $x \approx 4D$. The maximum for δu_0 is further downstream than the maximum for δv_0 because δu_0 is strongly affected by streamwise pressure gradients. The transverse velocity

https://doi.org/10.1017/jfm.2018.75 Published online by Cambridge University Press

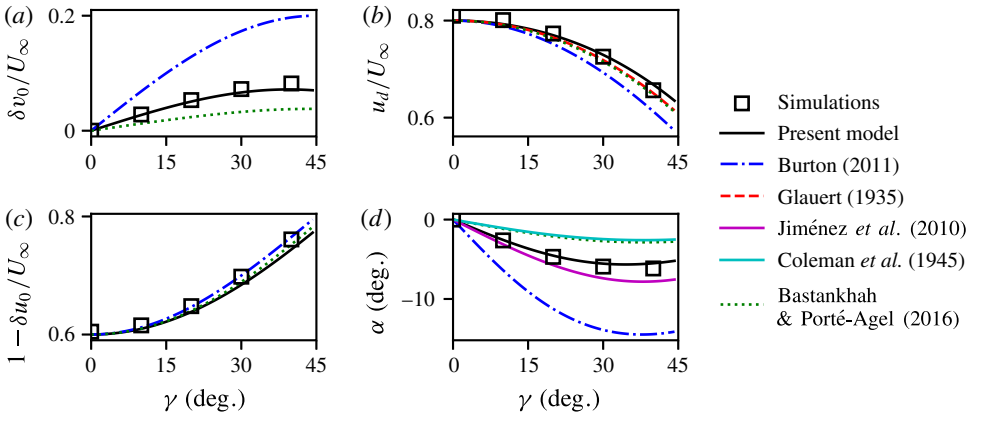


FIGURE 5. Comparison of (*a*) transverse velocity $\delta v_0/U_\infty$, (*b*) disk-averaged velocity u_d/U_∞, (*c*) streamwise velocity $1-\delta u_0/U_\infty$, and (*d*) skewness angle α measured in simulations with $C_T' = 1.0$ (squares) with present theory (solid black line) and prior models (other lines).

prediction (2.7) is expressed using the thrust coefficient $C_T = 16C_T'/(4 + C_T' \cos^2 \gamma)^2$ obtained from the induction factor (2.13). Predictions for several of the features of the inviscid region are provided by earlier models. Momentum theory (Burton *et al.* 2011) provides estimates for all quantities. Glauert's (1926) equation for the disk-averaged velocity was used by Coleman *et al.* (1945; Burton *et al.* 2011) to predict the skewness angle of the wake. Bastankhah & Porté-Agel (2016) recently used momentum conservation, the Bernoulli equation, and approximations to Glauert's and Coleman's equations to predict the streamwise and transverse velocities behind the disk. Jiménez *et al.* (2010) used momentum balance arguments to predict the initial wake deflection angle.

Figure 5 shows that the present inviscid region model accurately predicts the quantities measured in simulations. In contrast, the other models show significant disagreement in the skewness angle and transverse velocities. Momentum theory and Jiménez's equation overestimate the skewness angle and transverse velocity magnitudes. The skewness angle magnitude predicted by Coleman *et al.* (1945), and by extension the transverse velocity magnitude predicted by Bastankhah & Porté-Agel (2016), are approximately half as large as those obtained in the simulations. While Coleman's (1945) prediction may improve downstream as the wake is transformed by the counter-rotating vortex pair, this skewed elliptic vortex cylinder argument becomes less valid as a result of the curling.

3. Wake model for yawed turbines

An important application of the inviscid region theory described in the prior section is to determine an initial condition for models of the turbulent wake behind yawed turbines. We demonstrate the utility of the proposed inviscid region model by applying the predictions to the wake model of Shapiro *et al.* (2017), which we extend below to include yaw. As in Shapiro *et al.* (2017), the derivation includes possible time dependence (e.g. the turbine's local thrust coefficient and yaw angle could change over time). In this paper, however, we focus solely on the steady-state solution and compare it to the wind tunnel experiments of Bastankhah & Porté-Agel

https://doi.org/10.1017/jfm.2018.75 Published online by Cambridge University Press

(2016) that were performed under steady conditions. After neglecting the viscous terms, linearizing the advective term, i.e. $u_j\partial/\partial x_j = U_\infty\partial/\partial x$, and rewriting in terms of the mean velocity deficit $U_\infty\delta_{i1} - u_i(\boldsymbol{x}, t)$, the Reynolds averaged mean momentum equation becomes

$$\rho\frac{\partial}{\partial t}(U_\infty\delta_{i1} - u_i) + \rho U_\infty\frac{\partial}{\partial x}(U_\infty\delta_{i1} - u_i) = \frac{\partial p}{\partial x_i} - f_i + \frac{\partial\tau_{ij}}{\partial x_j}, \tag{3.1}$$

where $p(\boldsymbol{x}, t)$ is the pressure, $f_i(\boldsymbol{x}, t)$ is the turbine thrust force, and τ_{ij} the Reynolds stress tensor. The area of the wake downstream of the turbine expands due to turbulent mixing. If the expansion rate is determined only by the turbulence properties of the incoming flow, then the effective area of the wake $A(x)$ can be assumed to be a function of only the streamwise distance x from the turbine. Assuming that this effective area is known, the mean velocity deficit $\delta\boldsymbol{u}(x, t) = \delta u\,\boldsymbol{i} + \delta v\,\boldsymbol{j}$ is defined as

$$\delta u_i(x, t) = \frac{1}{A(x)}\int_{-\infty}^{\infty}\int_{-\infty}^{\infty}(U_\infty\delta_{i1} - u_i(x, y, z, t))\,\mathrm{d}y\,\mathrm{d}z. \tag{3.2}$$

Integrating (3.1) in the transverse directions yields

$$\frac{\partial}{\partial t}\left[\rho A(x)\delta u_i(x, t)\right] + U_\infty\frac{\partial}{\partial x}\left[\rho A(x)\delta u_i(x, t)\right] = \frac{\partial\bar{p}}{\partial x}\delta_{i1} - \bar{f}_i, \tag{3.3}$$

where $\bar{p}(x, t)$ and $\bar{f}_i(x, t)$ are the transversely averaged pressure and thrust force. Although the divergence of the Reynolds stress does not enter, the effects of turbulence are encoded in the modelled behaviour of $A(x)$.

Since the thrust force is confined to the rotor disk and the pressure gradient vanishes away from the turbine (Glauert 1935), the right-hand side of (3.3) only has to be considered in the region near the turbine rotor. The net effect of the pressure gradient and thrust force is therefore modelled as a source of momentum deficit $\partial\bar{p}/\partial x\,\delta_{i1} - \bar{f}_i = \rho A(x)\,S_i\,\delta(x)$, where S_i may be time dependent in cases of varying turbine thrust. Substituting into (3.3), expanding the spatial derivatives, and dividing by $\rho A(x)$ yields

$$\frac{\partial\delta u_i}{\partial t} + U_\infty\frac{\partial\delta u_i}{\partial x} = -w(x)\,\delta u_i(x, t) + S_i\,\delta(x), \tag{3.4}$$

where $w(x) = U_\infty A^{-1}(x)\,\mathrm{d}A/\mathrm{d}x$ is the wake expansion rate. To model the velocity deficit field in a smooth manner, the Dirac delta function in (3.4) is replaced by a normalized Gaussian function $G(x)$ with characteristic width $\Delta_w = R$. Furthermore, the wake area is written as $A(x) = d_w^2(x)\pi D^2/4$, where $d_w(x)$ is the effective diameter of the wake normalized by turbine diameter D defined by $d_w(x) = 1 + k_w\,\ln(1 + \exp[(x - 2\Delta_w)/R])$. This effective diameter $d_w(x)$ tends towards the Jensen (1983) model's linear expansion in the wake with expansion coefficient k_w, but stays above 1 and begins to expand only at $x \sim 2\Delta_w$ to prevent wake expansion within the zone of the Gaussian forcing. The velocity deficit source strengths, $S_1 = U_\infty\delta u_0$ and $S_2 = U_\infty\delta v_0$, are based on the inviscid model, where δu_0 and δv_0 are given by (2.12) and (2.7). This approach provides a smooth increase of the streamwise and transverse velocity deficits from zero upstream of the rotor to the desired 'wake initial condition' downstream of the rotor region.

The average streamwise velocity deficit $\delta u(x, t)$ is distributed using a Gaussian profile (Bastankhah & Porté-Agel 2014, 2016), which along $z = 0$ reads

$$u(x, y, t) = U_\infty - \delta u(x, t)\,\frac{D^2}{8\sigma_0^2}\,\exp\left(-\frac{(y - y_c(x, t))^2}{2\sigma^2(x)}\right), \tag{3.5}$$

https://doi.org/10.1017/jfm.2018.75 Published online by Cambridge University Press

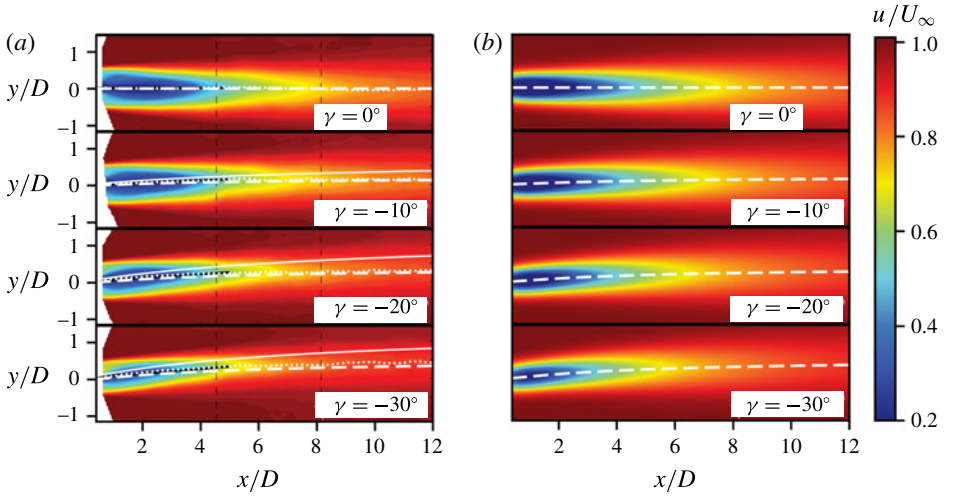


FIGURE 6. Hub-height colour contour plots of streamwise velocity as (*a*) measured in experiments (Bastankhah & Porté-Agel 2016) and (*b*) predicted using the proposed model. Measured centrelines of the wake (dotted) are compared to the model of Jiménez *et al.* (2010) (solid) and the present model (dashed). Experimental data in (*a*) adapted with permission from figure 3 of Bastankhah & Porté-Agel (2016).

where the width of the Gaussian $\sigma(x) = \sigma_0 d_w(x)$ is proportional to the effective normalized wake diameter with a proportionality constant σ_0. The velocity deficits are found by integrating (3.4), and the wake centreline $y_c(x, t)$ is found by integrating the transverse velocity according to

$$\frac{\partial y_c}{\partial t} + U_\infty \frac{\partial y_c}{\partial x} = -\delta v(x, t) \tag{3.6}$$

in the positive x direction subject to $y_c = 0$ far upstream of the turbine. The negative sign occurs because $\delta v(x, t)$ is a deficit in our sign convention. Equation (3.5) is consistent with (3.2); i.e. $\int_0^\infty (U_\infty - u) 2\pi\xi \, \mathrm{d}\xi = A(x)\delta u(x, t)$, where the distance $\xi = y - y_c(x, t)$ is measured from the wake centreline at $y_c(x, t)$.

The steady-state version of this wake model, where time derivatives vanish and the solution found by integrating in x and noting $G(x)d_w^2(x) \approx G(x)$,

$$\delta u(x) = \frac{\delta u_0}{d_w^2(x)} \frac{1}{2} \left[1 + \mathrm{erf}\left(\frac{x}{\Delta_w \sqrt{2}} \right) \right] \tag{3.7}$$

$$\delta v(x) = \frac{\delta v_0}{d_w^2(x)} \frac{1}{2} \left[1 + \mathrm{erf}\left(\frac{x}{\Delta_w \sqrt{2}} \right) \right] \tag{3.8}$$

$$y_c(x) = \int_{-\infty}^{x} \frac{-\delta v(x')}{U_\infty} \, \mathrm{d}x', \tag{3.9}$$

is compared to wind tunnel experiments by Bastankhah & Porté-Agel (2016). We use the experimental data for the unyawed ($\gamma = 0°$) case to fit the two required parameters k_w and σ_0, obtaining very reasonable values $k_w = 0.0834$ and $\sigma_0/D = 0.235$. The measured thrust coefficients of the rotating turbine (depending on the yaw angle, as reported in Bastankhah & Porté-Agel (2016)) are used to set the initial velocity deficits δu_0 and δv_0 in the model. Figure 6 compares the streamwise

https://doi.org/10.1017/jfm.2018.75 Published online by Cambridge University Press

velocity deficit at hub height for $\gamma = 0°$, $-10°$, $-20°$, and $-30°$. The centrelines of the measurements are compared to the present model and the model of Jiménez *et al.* (2010). The proposed model is found to be in excellent agreement with the experiments, particularly the estimate of the centreline of the wake.

4. Conclusion

Previous models for the inviscid region near a yawed actuator disk have generated conflicting predictions for the initial transverse velocity and skewness angle of the wake that fail to match actuator disk simulations. Accurate models for this inviscid region are vital for developing useful wake models for engineering design and control applications. In this paper, we derive a new model of the flow in the inviscid region near the disk. It treats the yawed actuator disk as an elliptically loaded lifting line and uses Prandtl's lifting line theory to determine the initial transverse velocity deficit and magnitude of the counter-rotating vortex pair shed from the yawed actuator disk. Momentum conservation and Bernoulli's equation are then applied to determine the disk-averaged velocity and streamwise velocity deficit. The predictions are found to agree with numerical simulations and accurately estimate the initial transverse velocity. We use the inviscid region predictions as initial conditions for a simple model of the turbulent flow field behind a yawed turbine and compare to experimental data. The newly proposed combined model for the inviscid and wake regions is remarkable for its simplicity and success at reproducing a variety of observations.

Acknowledgements

The authors thank L. A. Martínez for fruitful conversations and acknowledge funding from the National Science Foundation (grant CMMI 1635430). Computations made possible by the Maryland Advanced Research Computing Center (MARCC).

References

Aho, J., Buckspan, A., Laks, J., Fleming, P., Jeong, Y., Dunne, F., Churchfield, M., Pao, L. & Johnson, K. 2012 A tutorial of wind turbine control for supporting grid frequency through active power control. In *Proc. American Control Conf., Montreal, Canada*, pp. 3120–3131. IEEE.

Bastankhah, M. & Porté-Agel, F. 2014 A new analytical model for wind-turbine wakes. *Renew. Energy* **70**, 116–123.

Bastankhah, M. & Porté-Agel, F. 2016 Experimental and theoretical study of wind turbine wakes in yawed conditions. *J. Fluid Mech.* **806**, 506–541.

Branlard, E. & Gaunaa, M. 2015 Cylindrical vortex wake model: right cylinder. *Wind Energy* **18** (11), 1973–1987.

Branlard, E. & Gaunaa, M. 2016 Cylindrical vortex wake model: skewed cylinder, application to yawed or tilted rotors. *Wind Energy* **19** (2), 345–358.

Burton, T., Jenkins, N., Sharpe, D. & Bossanyi, E. 2011 *Wind Energy Handbook*. Wiley.

Calaf, M., Meneveau, C. & Meyers, J. 2010 Large eddy simulation study of fully developed wind-turbine array boundary layers. *Phys. Fluids* **22** (1), 015110.

Coleman, R. P., Feingold, A. M. & Stempin, C. W. 1945 Evaluation of the induced-velocity field of an idealized helicoptor rotor. *Tech. Rep.* NACA ARR No. L5E10.

Fleming, P., Gebraad, P., Lee, S., van Wingerden, J.-W., Johnson, K., Churchfield, M., Michalakes, J., Spalart, P. & Moriarty, P. 2015 Simulation comparison of wake mitigation control strategies for a two-turbine case. *Wind Energy* **18** (12), 2135–2143.

https://doi.org/10.1017/jfm.2018.75 Published online by Cambridge University Press

FRANDSEN, S., BARTHELMIE, R., PRYOR, S., RATHMANN, O., LARSEN, S., HØJSTRUP, J. & THØGERSEN, M. 2006 Analytical modelling of wind speed deficit in large offshore wind farms. *Wind Energy* **9** (1–2), 39–53.

GLAUERT, H. 1926 A general theory of the autogyro. *Tech. Rep.* H.M. Stationery Office.

GLAUERT, H. 1935 Division L: airplane propellers. In *Aerodynamic Theory*, pp. 169–360. Springer.

HANSEN, M. O. L. 2008 *Aerodynamics of Wind Turbines*, 2nd edn. Earthscan.

HOWLAND, M. F., BOSSUYT, J., MARTÍNEZ-TOSSAS, L. A., MEYERS, J. & MENEVEAU, C. 2016 Wake structure in actuator disk models of wind turbines in yaw under uniform inflow conditions. *J. Renew. Sust. Energy* **8** (4), 043301.

JENSEN, N. O. 1983 A note on wind generator interaction. *Tech. Rep.* Risø-M-2411.

JIMÉNEZ, A., CRESPO, A. & MIGOYA, E. 2010 Application of a LES technique to characterize the wake deflection of a wind turbine in yaw. *Wind Energy* **13** (6), 559–572.

MILNE-THOMSON, L. M. 1973 *Theoretical Aerodynamics*. Dover.

POPE, S. 2000 *Turbulent Flows*. Cambridge University Press.

SHAPIRO, C. R., BAUWERAERTS, P., MEYERS, J., MENEVEAU, C. & GAYME, D. F. 2017 Model-based receding horizon control of wind farms for secondary frequency regulation. *Wind Energy* **20** (7), 1261–1275.

STEVENS, R. J. A. M., GRAHAM, J. & MENEVEAU, C. 2014 A concurrent precursor inflow method for large eddy simulations and applications to finite length wind farms. *Renew. Energy* **68**, 46–50.

STEVENS, R. J. A. M., MARTÍNEZ, L. A. & MENEVEAU, C. 2018 Comparison of wind farm large eddy simulations using actuator disk and actuator line models with wind tunnel experiments. *Renew. Energy* **116** (Part A), 470–478.

https://doi.org/10.1017/jfm.2018.75 Published online by Cambridge University Press